MAX-DOAS observations of ship emissions in the North Sea

Anoop Mahajan, Liselotte Tinel, Véronique Riffault, Sarah Guilbaud, Barbara D'anna, Carlos Cuevas, Alfonso Saiz-Lopez

MAX-DOAS observations of ship emissions in the North Sea

Anoop S. Mahajan[1,2*], Liselotte Tinel[2], Véronique Riffault[2], Sarah Guilbaud[3], Barbara D'Anna[4], Carlos Cuevas[5] and Alfonso Saiz-Lopez[5]

[1]Indian Institute of Tropical Meteorology, Pune, India

[2]IMT Nord Europe, Institut Mines-Télécom, University of Lille, Centre for Energy and Environment, F-59000, Lille, France

[3]ATMO Hauts-de-France 59800 LILLE, France

[4] Université d'Aix-Marseille, CNRS, Laboratoire Chimie Environnement, Marseille, 13331, France

[5]Department of Atmospheric Chemistry and Climate, Institute of Physical Chemistry Blas Cabrera, CSIC, Madrid, Spain.

*Corresponding author: Anoop S. Mahajan (anoop@tropmet.res.in)

Keywords: NO_2; SO_2; MAX-DOAS, Coastal air quality.

Highlights:

- A month-long campaign shows that ship emissions in the North Sea usually have low sulphur content.
- In ship plumes, an increase in aerosol extinction coefficients, NO_2 and SO_2 was measured; HCHO did not increase every time.
- Land-based emissions dominate absolute concentrations of pollutants, but ship emissions contribute significantly to them.

Abstract

Shipping emissions were measured in Dunkirk, France. Elevated aerosol extinction coefficients (AEC), nitrogen dioxide (NO_2) and sulphur dioxide (SO_2) were observed up to 500 m from surface. Formaldehyde (HCHO) did not show an increase every time, which suggests that oxidation of emitted volatile organic compounds (VOCs) took longer than the transport to the observation path and dilution of direct emissions had occurred. Background NO_2, HCHO, and SO_2 levels were higher when the wind came over land or the surrounding industrial area, indicating that land-based sources contribute significantly; however, clear spikes in NO_2 and SO_2 were observed whenever ship plumes were sampled. Observations show that the ship emission contribution to pollution is significant, but land-based sources still dominate. The SO_2/NO_2 ratio was low throughout the campaign, although varying according to the ship type, confirming that the new fuel content regulations are being followed by most ships in this region.

1. Introduction

Shipping emissions can contribute significantly to air pollution, leading to degraded air quality and increased mortality, especially in coastal regions with significant maritime traffic (Corbett et al., 2008; Dalsøren et al., 2009; Endresen et al., 2008; Mifka et al., 2021). Shipping emissions include pollutants such as carbon dioxide (CO_2), carbon monoxide (CO), nitrogen oxides (NO_x), sulphur dioxide (SO_2), particulate matter such as $PM_{2.5}$ and PM_{10}, along with other volatile organic compounds (VOCs) and oxidised VOCs (OVOCs) (Eyring et al., 2007; Huszar et al., 2010; Matthias et al., 2016; Viana et al., 2014). These compounds can act as long-term greenhouse gases or affect air quality, posing serious health hazards (Endresen et al., 2008; Eyring et al., 2007; Gilgen et al., 2017; Viana et al., 2014). Indeed, in some areas in Europe with heavy ship traffic, shipping emissions can contribute as much as 80 % of the NOx and SO_2 in the environment (EEA, 2017). Particularly in urban harbour areas, where large vessels are docked in proximity to housing and city centres, this can significantly affect air quality (Lathwal et al., 2021; Tang et al., 2020; Viana et al., 2014). In these settings, shipping emissions can contribute to NO_x, SO_2 and PM levels comparable to road traffic at the urban scale (Mao et al., 2019; Merico et al., 2017).

Among the pollutants mentioned above, NO_x, SO_2, VOCs and OVOCs are reactive species which impact air quality. NOx can impact the oxidising capacity of the lower atmosphere by affecting the partitioning, production, and loss of free radical species (hydroxyl (OH), hydroperoxyl (HO_2), and peroxy (RO_2) radicals) and through the production of ozone (Crutzen, 1971, 1970; Stroud et al., 2003). SO_2, by contrast, can react with OH and form sulfuric acid (H_2SO_4), which can cause ecological damage and various health hazards (World Health Organization, 2021). SO_2 is also a precursor for sulphate aerosols, which are responsible for severe air pollution issues but have a cooling effect on climate (Twomey, 1977). Although several types of VOCs and OVOCs are emitted by ships, formaldehyde

(HCHO), the smallest carbonyl compound found in the atmosphere, can be used as a proxy for VOC emissions as it is directly emitted by combustion processes and is also an intermediate species formed by the oxidation of VOCs (Hak et al., 2005, and references therein). HCHO has been detected in shipping emissions using satellite data (Marbach et al., 2009). Once in the atmosphere, HCHO can photolyse and be oxidised by OH radicals, yielding HO_2 radicals and CO, affecting the global CO budget and the oxidative capacity of the atmosphere (Atkinson, 2000). It is also a crucial constituent in tropospheric O_3 formation, affecting air quality (Abbot, 2003; De Smedt et al., 2008).

The International Maritime Organisation (IMO) Marpol Annex VI has imposed since 2020 the maximum fuel sulphur content (FSC) for maritime traffic to be 0.50% S m/m worldwide. This global regulation is superposed by specific emission control areas (ECA), notably in the EU and the USA, where further emission restrictions on emissions of SOx and NOx from maritime traffic are enforced (Kattner et al., 2015). In ECA zones, such as the Baltic Sea and the North Sea in the EU, the maximum FSC is set to 0.10% S m/m. However, regular monitoring of these regulations is necessary, especially using independent techniques that do not rely on self-reporting by the shipping industry. Here, remote sensing techniques have an advantage as they can measure directly the exhaust plume of ships to quantify the SO_2 and NO_2 emissions from individual ships without mobilising complex (on-board) instrumentation and without dilution (Cheng et al., 2019; Seyler et al., 2017). Here, we report observations of shipping emissions of NO_2, SO_2 and HCHO using a multi-axis differential optical absorption spectrometer (MAX-DOAS) to quantify shipping emissions from a harbour in Dunkirk, France. The observations are used to identify relative increases in the concentrations of the three compounds along with the aerosol extinction coefficient (AEC) when sampling ship emissions and put in context with other sources in the region to assess the overall impact. We

also analyse the SO_2/NO_2 ratios to determine whether the ships are using low-sulphur fuels in accordance with regulations.

2. Methodology

Observations of atmospheric constituents along with various meteorological parameters were carried out as part of the joint 'SHIPping emission's contribution to AIR pollution in urban harbour area (SHIPAIR)' and 'Port Inventories in ReAl TimE' (PIRATE) campaigns. The field campaign was conducted from 31st August 2022 to 30th September 2022. A MAX-DOAS instrument was installed in the harbour of Dunkirk, France (51.009° N, 2.025° W) to study the profiles of trace gases in the ambient atmosphere and ship emissions (Figure 1). The instrument was placed on the rooftop of the Dunkirk-Great Britain ferry terminal at a height of 15 m above ground. The instrument was located approximately 300 m from the docking point of the most common ferries. Please note that the distance to the ship changes according to where the ship is when we measure the plume, which is not only when it is docked. The instrument was made of two parts: the first part consisted of a scanning telescope system, which had a light collector focused by a lens (focal length: 200 mm, diameter: 50.8 mm), and an indoor unit comprised of a spectrometer (Princeton Instruments SP500i) and a Charge-Coupled Device detector (Princeton Instruments Pixis 400B). The two units were connected by an optical fibre, transmitting scattered sunlight from the outside unit to the spectrometer. The spectrometer collected light in the spectral window between 296-383 nm. The instrument's electronic offset and dark current were measured regularly to correct the spectra, and the spectrometer was calibrated daily using mercury emission lines. The spectra were later also corrected using the Fraunhofer absorption lines in the solar spectrum.

DOAS analysis (Hönninger et al., 2004; Plane and Saiz-Lopez, 2006; Platt and Stutz, 2008) was used to retrieve the column densities of the oxygen dimer (O_4), NO_2, SO_2 and HCHO. In

this method, Rayleigh or Mie scattering is accounted for by a polynomial, and the remaining absorption contains narrow-band absorption from various chemical compounds. The optical densities of individual trace gases that absorb within the wavelength region are then identified using a least-squares fitting procedure. These are retrieved relative to the zenith spectrum, resulting in differential slant column densities (DSCD). The different absorption cross-sections used in the three fitting windows are given in Table 1. We used the QDOAS software (developed at BIRA-IASB, http://uv-vis.aeronomie.be/software/QDOAS/) (Fayt and Van Roozendael, 2013) for the DOAS retrievals.

The DSCDs were retrieved along 11 elevation viewing angles (0°, 1°, 2°, 3°, 4°, 5°, 7°, 10°, 15°, 20°, 90°). The instrument azimuth viewing direction was changed three times during the campaign (Figure 1). The first light path pointed westward (azimuth 262°) north of the ferry dock from 1st to 12th September 2022, the second light path looked across the harbour opening towards the open ocean (azimuth 306°) from 12th to 20th September 2022 and 28th to 29th September 2022, and the third path looked across an industrial area to the east of the harbour (azimuth 60°) from 20th to 28th September 2022. This made it possible to identify ship emissions and other sources due to local industrial emissions during the campaign. The path length of MAX-DOAS is not constant but changes depending on the local conditions such as the ambient aerosol loading. The path length ranged between 3 km and 30 km during the campaign, and the O_4 observations were used to correct the effect of the path length on the other trace gas mixing ratio estimations. This correction was done using a radiative transfer model with a profile retrieval algorithm as detailed below.

To retrieve the volume mixing ratios from the DSCDs, we used a profile retrieval algorithm in conjunction with a radiative transfer model. The current study used the Mainz profile algorithm (MAPA) (Beirle et al., 2019) to calculate the AEC and mixing ratio profiles. The profile retrieval consists of two parts. The first part is retrieving the AEC profile using the O_4

DSCDs, and the second part is retrieving the trace gas profiles using the retrieved aerosol profiles. Both parts consist of the same steps: a forward model and an inversion algorithm (MAPA). The forward model used is the Monte Carlo Atmospheric Radiative Transfer Inversion Model (McArtim) (v1) (Deutschmann et al., 2011). The retrieved mixing ratios are then subjected to a quality check and quality control according to various flags to ensure that the resulting data are valid. Further details of MAPA, the flags used to identify valid data (in addition to filtering faulty estimations due to multiple scattering caused by clouds), and the thresholds for the various quality check flags can be found in Beirle et al. (2019).

Ancillary observations of meteorological parameters were made during the campaign. Figure 2 shows the time series of wind speed, wind direction, temperature, and relative humidity throughout the campaign. In order to identify long-distance sources and their impact on the background levels of pollutants, we also analysed the air mass back trajectories arriving at the measurement site. They were calculated using the HYSPLIT model (Draxler and Hess, 1998; Stein et al., 2015) GDAS 1° × 1° (3-hour time resolution) meteorological data, . The trajectories were run for -72 hours (3 days) and arrived at the site at half the height of the planetary boundary layer. Five clusters were identified from the trajectories: 1) SW air masses mainly passing over continental France, 2) SSW air masses mostly passing over the Atlantic Ocean, 3) NW air masses passing over the English Channel and the UK, 4) N air masses passing over the English Channel and the UK, and 5) NE air masses passing over the North Sea. Examples of cluster averages and time series of air masses from each cluster are shown in Figure 3.

During the campaign, a total of 520 vessels entered the harbour, of which 350 were ferries (day and night). During the daytime, when the MAX-DOAS was sampling, 151 ferries entered the harbour throughout the campaign. For the periods when the DOAS was pointed toward the harbour, there were 169 ships, of which 110 were ferries. This shows that the

main drawback of the MAX-DOAS is that it can only sample during the daytime and would, therefore, miss some vessels.

3. Results and discussion

3.1 Meteorological Conditions

Figure 3 shows the air mass back trajectory clusters observed during the campaign according to the different light paths. During observations along light path 1 (azimuth 262°), the trajectories mainly were from clusters 1-3 in three distinct periods, corresponding to air masses with a continental influence. This light path is pointed just north of the ferry dock and should have the maximum direct emissions in the path when the ferry ships are docked. However, the local wind direction during this period varied with some instances of marine winds (NW-NE), with low contributions of local emissions from the city of Dunkirk and surrounding regions, along with periods of S, SE and SW winds, when the air mass passed over land before reaching the site (Figure 2). During observations along light path 2 (towards the north over the open sea), a mix of air masses from all 5 clusters was observed (Figure 3). The local wind direction was either NW or NE, with wind speeds increasing towards the end of the measurement period along this light path (Figure 2). During observations along light path 3 (pointing towards the industrial area east of the measurement site), the air masses were from clusters 1, 3-5. Thus, air masses passing over the Atlantic Ocean were not sampled (Figure 3). The local wind direction shows that the air initially came from the NW, over the open sea, but then gradually shifted across the south to eventually come from the NE (Figure 2). Thus, emissions from the Dunkirk suburban areas of Loon-Plage and Grande-Synthe and local industries were observed when the winds came from the south. The wind speed gradually increased during the light path 3 period, similar to light path 2. Finally, the temperature decreased gradually throughout the campaign as autumn arrived. The relative

188 humidity (RH) was variable, with periods of high RH most of the campaign, followed by low
189 RH when the wind speed was high (Figure 2). During the campaign, there were periods of
190 rain, which were flagged by the DOAS data and excluded from further analysis.
191
192 **3.2 Differential Slant Column Densities**
193 Figure 4 shows the O_4, NO_2, HCHO and SO_2 DSCDs observed throughout the campaign. The
194 O_4 DSCDs show a considerable variation depending on the meteorological conditions. This is
195 due to a change in the aerosol loading, which strongly affects the total observable path length.
196 The O_4 DSCDs show a decreasing gradient with increasing elevation angles, which shows
197 that most of the aerosols are concentrated in the boundary layer. There were periods when the
198 O_4 DSCDs fell much lower than usual, which coincided with rain events, as confirmed by
199 visual images from a CCTV camera installed at the measurement site. As expected, visibility
200 is much lower during rain events. This data was filtered from further analysis as it can affect
201 the radiative transfer calculations due to multiple scattering. Examples of typical days when
202 changes in O_4 DSCDs along different elevation angles, and hence aerosol concentrations, can
203 be observed during ship docking periods are shown in Figure 5.
204 DSCD time series for O_4, NO_2, HCHO, and SO_2 are also shown in Figure 4. NO_2 DSCDs are
205 observed above the detection limit on all days of the campaign, but HCHO and SO_2 are more
206 intermittent. Interestingly, NO_2 and HCHO show higher DSCDs at lower elevation angles
207 most of the time, showing a decreasing vertical profile, but SO_2 is not always as clear, with
208 some instances of higher SO_2 at higher elevation angles. This indicates that there are periods
209 when SO_2 is below the detection limit in the lowest layer but is present as a lofted layer
210 higher than 100 m. This would occur when the background SO2 is low, but ship exhaust
211 emits SO_2 directly above the surface. The same vertical profile was also observed when a
212 significant increase in SO_2 was observed on 21st September, when the instrument was

observing along light path 3, towards the industrial area to the east of the measurement site. In this case, SO_2 was emitted from a chimney and was therefore also observed as a lofted layer.

Figure 5 provides a zoom-in on two typical days when these different trace gas gradients are visible, showing the O_4, NO_2, HCHO and SO_2 DSCDs along different elevation angles on 12th and 19th September 2022, when the instrument was pointing north over the North Sea along light path 2. Apparent differences can be seen in the O_4, NO_2, HCHO, and SO_2 DSCDs. The DSCDs were higher on 12th September as compared to 19th September. The local wind direction was similar on both days, but the wind speed was much lower on 12th September. However, the air mass trajectories were very distinct, with cluster 1 air masses, which passed over land, observed on 12th September, and clusters 4 and 5, which passed over the North Sea, observed on 19th September. Thus, in addition to ship emissions, which led to peaks in all species on both days, the background levels are dominated by other emissions. This shows that meteorological conditions determine the absolute concentration of pollutants at the measurement site.

3.3 Aerosol Extinction Coefficients and Trace Gas Mixing Ratios

Figure 6 shows the vertical profiles of AEC and NO_2, HCHO and SO_2 mixing ratios. Periods of high aerosol loading can be clearly seen in the AEC profiles, including periods with clouds, which show high AEC across the entire profile during these periods. These periods were filtered unless they passed the MAPA filters. It should be noted that clouds can introduce additional uncertainties on the retrieval of trace gas mixing ratios from the DSCDs, and some of the cloudy periods pass the MAPA filters, which are designed to avoid clouds (check Methodology). These periods are clearly identifiable with elevated AEC and trace gas mixing ratios at higher altitudes (Figures 6 and 8). In theory, while the AEC can be directly

attributed to the presence of clouds, the retrieved trace gas mixing ratios account for the multiple scattering due to clouds and hence should be valid. Unfortunately, this is not always the case due to non-linear multiple scattering effects which are still not well characterized in radiative transfer models, and hence the elevated trace gas concentrations at higher altitudes should be treated with caution (Beirle et al., 2019). However, the presence of clouds does not directly affect the trace gas retrievals at lower altitudes (<500 m) and, hence, we have high confidence in the measurements showing elevated concentrations near the surface, which correlate with the presence of ships. There are several periods of high AEC, even under clear sky conditions, where the AEC increases to higher values (>0.4 km^{-1}) up to 500 m from the surface. These periods coincide with increases in NO_2, SO_2, and sometimes, HCHO. In the case of NO_2, while background mixing ratios of 2-5 ppbv are observed, distinct peaks of up to >40 ppbv are measured intermittently when the ships are in the harbour. HCHO mixing ratios show higher average background mixing ratios up to altitudes of ~1 km but also show peaks of >15 ppbv up to 500 m during periods of ship activity in the harbour. The peaks in HCHO are not observed every time the ship is in the harbour, unlike NO_2, which is highly regular, suggesting that in addition to ship emissions, local emissions leading to the formation of HCHO also control the observed HCHO mixing ratios. As HCHO depends on anthropogenic and natural sources, the increase in HCHO is not expected to be always observable above the background due to a lower impact on the signal-to-noise. In the case of SO_2, peaks of >10 ppbv are often observed when the ships are in the harbour, showing that ship emissions still contribute to the SO_2 loading near Dunkirk. However, the highest peak in SO_2 was observed on 21st September 2022 (Figure 6), when the instrument was observing along light path 3, which pointed towards the industrial area east of the harbour. This increase in SO_2 also did not coincide with the timing of ships in the harbour, confirming that the emissions were from the industrial area, which houses a steel plant with three coal-fired blast

furnaces and a total annual production capacity of 7 million tons. As this was an intermittent emission, it is most likely to have come from the blast furnaces at the steel plant (Setyan et al., 2019; Zhang et al., 2021).

Figure 7 shows the time series of surface (averaged over the lowest 200 m) AEC and trace gas mixing ratios throughout the campaign. Higher background levels were observed on some days compared to others. This is especially noticeable when the air masses from sectors 4 and 5 travel over the North Sea and show low values for all pollutants, apart from some peaks during the periods when the ship plumes were sampled, e.g., 14th-20th September and 24th-26th September (Figure 3). However, on other days, a spike above the background is observed whenever the ship emissions are sampled. These spikes were observed almost daily for AEC, NO_2 and SO_2. The increase in HCHO is not as apparent, which indicates that the lifetime of VOCs emitted by ships is longer than the transport time to and within the light path and that primary emissions of HCHO from the ship stacks are diluted before measurement. The change in background over the campaign suggests that sources other than ship emissions control the average pollutant levels over the measurement site, but ship emissions still contribute to the observed increase in pollutants. Previous studies have reported similar observations in the German Blight near Hamburg (Seyler et al., 2017) and in Shanghai (Cheng et al., 2019), concluding that ship emissions' contribution to pollution levels is large, but land-based sources still control the overall pollution loading.

Figure 8 shows a zoomed-in example of the vertical profiles for two days (12th and 19th of September 2022), which were observed along light path 2 as mentioned above, but with air masses coming from cluster 1 (over land) or clusters 4-5 (over sea). The large difference in the background mixing ratios, especially for NO_2 and HCHO, can be seen, with higher mixing ratios observed when the air masses arrived from cluster 1 (over land) on 12th September. On this day, apparent increases in NO_2 are observed at regular intervals, which

can be attributed to the presence of ferries in the harbour. NO_2 and SO_2 show a significant increase in the morning when the ships are in the harbour, but the subsequent increases in the afternoon are smaller as compared to the morning. This was due to two reasons: 1) the wind speed was much lower in the morning, implying slower dispersion of ship emissions (note that no relationship between wind speed and observed concentrations is seen when the full campaign data is considered), and 2) differences in local wind direction. Indeed, in the morning, the wind was blowing directly from the north, towards the DOAS light path for ships approaching or leaving the harbour, compared to the afternoon when the wind was blowing from the south, advecting emissions from ships inside the harbour and continental sources to the DOAS light path. This change is also visible in the HCHO mixing ratios, which are lower in the morning but increase throughout the day due to diurnal photochemistry and the fact that the instrument sampled air masses with higher VOCs from the land in the afternoon. On 19th September, spikes in NO_2 and SO_2 were still visible when ships were in the harbour but considering that we were sampling clean marine air masses and that the wind speed was higher than on 12th September, the peaks are shorter lived as the pollutants are advected and dispersed more rapidly. In fact, SO_2 is below the detection limit for most of the day, with only a few instances observed above the detection limit. Note that the morning of the 19th of September was cloudy, which can be seen in the AEC observations and was confirmed using concurrent CCTV images. Even during cloudy conditions, the enhancement in trace gases is observed close to the surface in the MAX-DOAS profiles.

Figure 9 shows a comparison of the vertical profiles of the AEC, the NO_2 and SO_2 mixing ratios, and the corresponding O_4, NO_2 and SO_2 DSCDs when the MAX-DOAS sampled ship emissions, as well as instances when it sampled background air, all on 12th September, selected for similar wind speed and wind direction. This was a ‘clear sky’ day, and the sky conditions were verified using independent CCTV images that were collected concurrently

throughout the campaign. An increase in all parameters can be observed in the lower boundary layer when the ship plume was sampled (Figure 9). It should be noted that DOAS observes the concentrations along a light path, and the change in mixing ratios is averaged over the entire path length. The increase due to ship emissions is localised rather than averaged; hence, the increase in mixing ratios corresponds to a lower limit. The increase in DSCDs is more representative of the total increase in pollutants, although, with a MAX-DOAS, it is not possible to identify increases only in the air masses with the plume; hence, MAX-DOAS measurements cannot provide emission estimates from individual ships. However, this inherent drawback is compensated for by the fact that these observations provide remote sensing data that allow statistical analysis of signals at different altitudes from thousands of ships at a distance and under various environmental conditions, which is not possible with in situ observations. It should also be noted that this campaign was conducted over a short period of time to test the capability of the MAX-DOAS to measure ship plumes. While the observations qualitatively demonstrate this capability, the lack of long-term observations inhibits a detailed statistical analysis to calculate emission factors due to changing meteorological conditions. A longer dataset would be needed in the future for a more quantitative analysis and characterise individual ship emissions.

3.4 In situ observations of trace gases

Figure 10 shows the time series of the surface NO2 and SO2 mixing ratios observed by the in situ sensors throughout the campaign. In general, the in situ sensors reported higher mixing ratios than the MAX-DOAS instrument. This is not surprising considering the fact that the MAX-DOAS data represent averaged concentrations along the light path, and the surface value is indicative of an average over the lowest 200 m. The path length varied throughout the campaign depending on the environmental conditions, but the retrieved mixing ratio takes

the difference in the light path into account. However, it does not account for the heterogeneity in emissions along the different light paths, which can affect the average mixing ratios. The in situ sensors were also able to observe several peaks throughout the campaign but did not observe systematically the same plumes as the MAX-DOAS instrument. Indeed, a comparison between the in situ and MAX-DOAS observations shows a poor match (Figure 10). There are several occasions when the MAX-DOAS sees higher values of NO_2 and SO_2, suggesting that it is sampling the ship plume while the in situ sensors do not show an increase. On some occasions, the in situ sensors detect an increase, which is not reflected in the MAX-DOAS observations. This shows that both instruments sampled different ship plumes, depending on the position of the ships and the wind direction. The in situ sensors also observed plumes for very short periods (1 m or shorter) most of the time, especially when the wind direction was coming from over the docking station when the ships were in the harbour. By contrast, the MAX-DOAS was able to observe plumes for longer periods (considering an elevation angle sequence of 10 minutes). This is because of the longer light path, which increases the probability of sampling the ship's plumes when it is close to the harbour. Thus, a direct comparison between the in situ sensors and the MAX-DOAS is not possible here, as the number of plumes observed in common is very low and the integrated observation times very different (2-4 mins for in situ and 10 mins for DOAS). For a detailed comparison, a longer measurement campaign needs to be conducted and the discrepancy between the MAX-DOAS and in situ sampling periods needs to be addressed, by increasing the temporal resolution of the MAX-DOAS observations… . The observations show the importance of having different measurement systems to increase the likelihood of monitoring ship emissions as both methods have their own advantages, although characterisation of each method still remains a challenge.

3.5 SO_2/NO_2 ratio

While the MAX-DOAS does not directly allow the estimation of the NO_2 and SO_2 emission factors, the SO_2/NO_2 concentration ratios can be used to estimate whether ships are using low-sulphur fuels to track compliance (Cheng et al., 2019; Seyler et al., 2017). This method was already used as early as 2012 by McLaren et al. (2012), who employed an active long-path DOAS technique to measure the SO_2/NO_2 ratios in ship plumes and suggested that high ratios were a result of high sulphur content in marine fuels. In Shanghai, the SO_2/NO_2 ratio exceeded 2 for the high sulphur emitting ships (Cheng et al., 2019), while in the German Blight close to Hamburg, the ratio for high sulphur fuelled ships was close to 0.35 (this value was similar to (McLaren et al., 2012)). The median ratio for low sulphur fueled ships was 0.058 (Seyler et al., 2017). Figure 11 shows the surface SO_2/NO_2 ratio observed during the measurement campaign and the recorded ship arrival times into the harbour by the MAX-DOAS (bottom 200 m) and the in situ analysers. Not all ships stayed for the same duration, and their engines were on for variable periods. Therefore, the arrival times are indicative of ship emissions but do not cover the entire period when the MAX-DOAS or the in situ instruments sampled the ship plume. Typically, the ferries stayed in the port for 20-30 minutes, during which a change in the SO_2/NO_2 ratio can be detected. An increase in the ratio is observed in the MAX-DOAS every time a ship enters the harbour but not in the in situ observations, which see an increase only sometimes. This is expected as the MAX-DOAS observations are path-averaged concentrations, which increases the likelihood of it sampling the ship plume. By contrast, the in situ instrument is extremely sensitive to the local wind direction and hence samples only a fraction of the total number of ships. The relative increase in the MAX-DOAS observations also depends on the background conditions and the meteorological conditions, in addition to the ship arrival times. Hence, it was not possible to draw any clear conclusion on the emission factors for individual ships, and a larger sample

size is needed. For the present campaign, the ratio ranged between 0 and 2, with most ferry-based plumes showing a ratio between 0.15 and 0.3, depending on the environmental conditions. The SO_2/NO_2 ratio observed here is much higher than in the German Blight (Seyler et al., 2017). We are not sure of the reason behind this, but it could be due to the engine regime and/or related to the distance between the ship plumes and the measurement site. Considering that we were located at the harbour, we were mainly measuring 'cold' emissions or auxiliary motor regimes. It could also be related to the proximity to the ship emissions, which leads to direct measurement of the plumes, which the previous DOAS-based studies did not have. The study by Seyler et al. (2017), for example, sampled plumes from a distance of 3 km for a longer measurement period. Hence, the difference in the observed ratios is not surprising.

The ratio suggests that the sulphur content of the ship fuel was higher than sources contributing to the background levels of pollutants, as observed hitherto in the Strait of Georgia (McLaren et al., 2012). However, there are instances when the SO_2/NO_2 ratio is as high as 0.8. Hence, it looks probable that a few ships did not adhere to the low sulphur fuel regulations. Note that the high ratios on 21st September coincide with SO_2 emissions from the industrial area, which results in a significant amount of SO_2 above the typically observed ship emissions (Figure 11). The observed SO_2/NO_2 ratio variation suggests some non-conformance with the enforced sulphur limitation. Thus, MAX-DOAS measurements can provide valuable observations to identify the compliance of fuel sulphur content usage in ship plumes.

4. Conclusions

Ship emissions were investigated at the Dunkirk harbour in September 2022 using the MAX-DOAS instrument. Elevated levels of aerosol extinction coefficients, NO_2 and SO_2 were

observed whenever the instrument sampled emissions from the ship. HCHO, by contrast, was not observed in each ship plume, suggesting that, at times, the sampling timescale was lower than the atmospheric oxidation lifetime of VOCs that can lead to HCHO formation but also large enough for dilution of direct HCHO emissions. While spikes were clearly detected when vessels were entering or leaving the harbour, the background levels were controlled by local and long-range transport rather than ship emissions. Hence, the local air quality is not determined by the shipping sources but instead by local and regional ones. We also used the SO_2/NO_2 ratio to determine whether the ships were compliant with the 2020 FSC regulations, and observations showed that while most ships had low SO_2/NO_2 ratios, there were several instances when a high SO_2/NO_2 ratio was observed, suggesting that some ships are still not compliant with the new regulations. However, it is important to note that this campaign provides only some evidence for this, and a longer dataset is needed make a conclusive statement on the adherence to the new regulations considering the higher background of the measured pollutants at this site.

5. Acknowledgements

The authors thank all the participants involved in the SHIPAIR (ANR-21-CE22-0015 SHIPAIR) and PIRATE (ADEME grant 2166D0028) campaign in Dunkirk for their support throughout the study. The authors gratefully acknowledge the NOAA Air Resources Laboratory (ARL) for providing the HYSPLIT transport and dispersion model. The Indian Institute of Tropical Meteorology is funded by the Ministry of Earth Sciences, Government of India. IMT Nord Europe acknowledges financial support from the Labex CaPPA project, which is funded by the French National Research Agency (ANR) through the PIA (Programme d'Investissement d'Avenir) under contract ANR-11-LABX-0005-01, and the CLIMIBIO and ECRIN projects, all financed by the Regional Council "Hauts-de-France" and

the European Regional Development Fund (ERDF). ASM's research stay at IMT Nord Europe was supported by the Labex CaPPA.

CRediT authorship contribution statement

Anoop S.Mahajan: Conceptualization, Data curation, Formal analysis, Funding acquisition, Investigation, Methodology, Supervision, Visualization, Writing – original draft, Writing – review & editing. Liselotte Tinel: Conceptualization, Data curation, Formal analysis, Funding acquisition, Writing – original draft, Writing – review & editing. Veronique Riffault: Conceptualization, Funding acquisition, Project administration, Writing – review & editing. Sarah Guilbaud: Data curation, Investigation, Methodology, Validation. Barbara D'Anna: Conceptualization, Funding acquisition, Project administration, Writing – review & editing. Carlos Cuevas: Methodology, Project administration, Writing – review & editing. Alfonso Saiz-Lopez: Funding acquisition, Investigation, Methodology, Resources, Writing – review & editing.

Declaration of competing interest

The authors declare that they have no known competing financial interests or personal relationships that could have appeared to influence the work reported in this paper.

Data availability

Data will be made available on request.

6. References

Abbot, D.S., 2003. Seasonal and interannual variability of North American isoprene emissions as determined by formaldehyde column measurements from space. Geophys. Res. Lett. 30, 1999–2002. https://doi.org/10.1029/2003GL017336

Atkinson, R., 2000. Atmospheric chemistry of VOCs and NO(x). Atmos. Environ. 34, 2063–2101. https://doi.org/10.1016/S1352-2310(99)00460-4

Beirle, S., Dörner, S., Donner, S., Remmers, J., Wang, Y., Wagner, T., 2019. The Mainz profile algorithm (MAPA). Atmos. Meas. Tech. 12, 1785–1806. https://doi.org/10.5194/amt-12-1785-2019

Bogumil, K., Orphal, J., Homann, T., Voigt, S., Spietz, P., Fleischmann, O.C., Vogel, A., Hartmann, M., Kromminga, H., Bovensmann, H., Frerick, J., Burrows, J.P., 2003. Measurements of molecular absorption spectra with the SCIAMACHY pre-flight model: instrument characterization and reference data for atmospheric remote-sensing in the 230–2380 nm region. J. Photochem. Photobiol. A Chem. 157, 167–184. https://doi.org/10.1016/S1010-6030(03)00062-5

Chance, K., Kurucz, R.L., 2010. An improved high-resolution solar reference spectrum for earth's atmosphere measurements in the ultraviolet, visible, and near infrared. J. Quant. Spectrosc. Radiat. Transf. 111, 1289–1295. https://doi.org/10.1016/j.jqsrt.2010.01.036

Cheng, Y., Wang, S., Zhu, J., Guo, Y., Zhang, R., Liu, Y., Zhang, Y., Yu, Q., Ma, W., Zhou, B., 2019. Surveillance of SO₂ and NO₂ from ship emissions by MAX-DOAS measurements and the implications regarding fuel sulfur content compliance. Atmos. Chem. Phys. 19, 13611–13626. https://doi.org/10.5194/acp-19-13611-2019

Corbett, J.J., Winebrake, J.J., Lauer, A., 2008. Mortality from Ship Emissions : A Global Assessment Mortality from Ship Emissions : A Global Assessment. Environ. Sci. Technol 41, 8512–8518. https://doi.org/10.1021/es071686z

Crutzen, P.J., 1971. Ozone production rates in an oxygen-hydrogen-nitrogen oxide atmosphere. J. Geophys. Res. 76, 7311–7327. https://doi.org/10.1029/JC076i030p07311

Crutzen, P.J., 1970. The influence of nitrogen oxides on the atmospheric ozone content. Q. J. R. Meteorol. Soc. 96, 320–325.

Dalsøren, S.B., Eide, M.S., Endresen, O., Mjelde, A., Gravir, G., Isaksen, I.S.A., 2009.

Update on emissions and environmental impacts from the international fleet of ships: The contribution from major ship types and ports. Atmos. Chem. Phys. 9, 2171–2194. https://doi.org/10.5194/acp-9-2171-2009

De Smedt, I., Müller, J.-F., Stavrakou, T., van der A, R., Eskes, H., Van Roozendael, M., 2008. Twelve years of global observations of formaldehyde in the troposphere using GOME and SCIAMACHY sensors. Atmos. Chem. Phys. 8, 4947–4963. https://doi.org/10.5194/acp-8-4947-2008

Deutschmann, T., Beirle, S., Frieß, U., Grzegorski, M., Kern, C., Kritten, L., Platt, U., Prados-Román, C., Pukite, J., Wagner, T., Werner, B., Pfeilsticker, K., 2011. The Monte Carlo atmospheric radiative transfer model McArtim: Introduction and validation of Jacobians and 3D features. J. Quant. Spectrosc. Radiat. Transf. 112, 1119–1137. https://doi.org/10.1016/j.jqsrt.2010.12.009

Draxler, R.R., Hess, G.D., 1998. An Overview of the HYSPLIT_4 Modelling System for Trajectories, Dispersion, and Deposition. Aust. Meteorol. Mag. 47, 295–308.

EEA, 2017. The impact of international shipping on European air quality and climate forcing. https://doi.org/10.2800/4907

Endresen, O., Eide, M., Dalsoren, S., Isaksen, I.S., Sorgard, E., 2008. The Environmental Impacts of Increased International Maritime Shipping. Glob. Forum Transp. Environ. a Glob. World 1–43.

Eyring, V., Corbett, J.J., Lee, D.S., Winebrake, J.J., 2007. Brief summary of the impact of ship emissions on atmospheric composition, climate, and human health. Doc. Submitt. to Heal. Environ. Sub-gr. Int. Marit. Organ. i, 7.

Fayt, C., Van Roozendael, M., 2013. QDOAS 1.00. Software User Manual [WWW Document]. URL http://uv-vis.aeronomie.be/software/QDOAS/

Fleischmann, O.C., Hartmann, M., Burrows, J.P., Orphal, J., 2004. New ultraviolet

absorption cross-sections of BrO at atmospheric temperatures measured by time-windowing Fourier transform spectroscopy. J. Photochem. Photobiol. A Chem. 168, 117–132. https://doi.org/https://doi.org/10.1016/j.jphotochem.2004.03.026

Gilgen, A., Ting, W., Huang, K., Ickes, L., Neubauer, D., Lohmann, U., 2017. How important are future marine and shipping aerosol emissions in warming Arctic summer and autumn? Atmos. Chem. Phys. Discuss. 2017, 1–41. https://doi.org/10.5194/acp-2017-1007

Hak, C., Pundt, I., Trick, S., Kern, C., Platt, U., Dommen, J., Ordóñez, C., Prévôt, A.S.H., Junkermann, W., Astorga-Lloréns, C., Larsen, B.R., Mellqvist, J., Strandberg, A., Yu, Y., Galle, B., Kleffmann, J., Lörzer, J.C., Braathen, G.O., Volkamer, R.A., W. Junkermann, 2005. Intercomparison of four different in-situ techniques for ambient formaldehyde measurements in urban air. Atmos. Chem. Phys. 5, 2881–2900.

Hönninger, G., von Friedeburg, C., Platt, U., 2004. Multi axis differential optical absorption spectroscopy (MAX-DOAS). Atmos. Chem. Phys. 4, 231–254. https://doi.org/10.5194/acp-4-231-2004

Huszar, P., Cariolle, D., Paoli, R., Halenka, T., Belda, M., Schlager, H., Miksovsky, J., Pisoft, P., 2010. Modeling the regional impact of ship emissions on NOx and ozone levels over the Eastern Atlantic and Western Europe using ship plume parameterization. Atmos. Chem. Phys. 10, 6645–6660. https://doi.org/10.5194/acp-10-6645-2010

Kattner, L., Mathieu-Üffing, B., Burrows, J.P., Richter, a., Schmolke, S., Seyler, a., Wittrock, F., 2015. Monitoring compliance with sulfur content regulations of shipping fuel by in situ measurements of ship emissions. Atmos. Chem. Phys. 15, 10087–10092. https://doi.org/10.5194/acp-15-10087-2015

Lathwal, P., Vaishnav, P., Morgan, M.G., 2021. Environmental and health consequences of shore power for vessels calling at major ports in India. Environ. Res. Lett. 16.

https://doi.org/10.1088/1748-9326/abfd5b

Mao, X., Chen, C., Comer, B., Rutherford, D., (ICCT), I.C. on C.T., 2019. Cost and Benefits of a Pearl River Delta Emission Control Area.

Marbach, T., Beirle, S., Platt, U., Hoor, P., Wittrock, F., Richter, A., Vrekoussis, M., Grzegorski, M., Burrows, J.P., Wagner, T., 2009. Satellite measurements of formaldehyde linked to shipping emissions. Atmos. Chem. Phys. 9, 8223–8234.

Matthias, V., Aulinger, A., Backes, A., Bieser, J., Geyer, B., Quante, M., Zeretzke, M., 2016. The impact of shipping emissions on air pollution in the greater North Sea region-Part 2: Scenarios for 2030. Atmos. Chem. Phys. 16, 759–776. https://doi.org/10.5194/acp-16-759-2016

McLaren, R., Wojtal, P., Halla, J.D., Mihele, C., Brook, J.R., 2012. A survey of NO2:SO2 emission ratios measured in marine vessel plumes in the Strait of Georgia. Atmos. Environ. 46, 655–658. https://doi.org/10.1016/J.ATMOSENV.2011.10.044

Meller, R., Moortgat, G.K., 2000. Temperature dependence of the absorption cross sections of formaldehyde between 223 and 323 K in the wavelength range 225-375 nm. J. Geophys. Res. 105, 7089–7101.

Merico, E., Gambaro, A., Argiriou, A., Alebic-Juretic, A., Barbaro, E., Cesari, D., Chasapidis, L., Dimopoulos, S., Dinoi, A., Donateo, A., Giannaros, C., Gregoris, E., Karagiannidis, A., Konstandopoulos, A.G., Ivošević, T., Liora, N., Melas, D., Mifka, B., Orlić, I., Poupkou, A., Sarovic, K., Tsakis, A., Giua, R., Pastore, T., Nocioni, A., Contini, D., 2017. Atmospheric impact of ship traffic in four Adriatic-Ionian port-cities: Comparison and harmonization of different approaches. Transp. Res. Part D Transp. Environ. 50, 431–445. https://doi.org/https://doi.org/10.1016/j.trd.2016.11.016

Mifka, B., Žurga, P., Kontošić, D., Odorčić, D., Mezlar, M., Merico, E., Grasso, F.M., Conte, M., Contini, D., Alebić-Juretić, A., 2021. Characterization of airborne particulate

563 fractions from the port city of Rijeka, Croatia. Mar. Pollut. Bull. 166, 112236.
564 https://doi.org/10.1016/J.MARPOLBUL.2021.112236
565 Plane, J.M.C., Saiz-Lopez, A., 2006. UV-Visible Differential Optical Absorption
566 Spectroscopy (DOAS), in: Heard, D.E. (Ed.), Analytical Techniques for Atmospheric
567 Measurement. Wiley-Blackwell, Oxford, UK, pp. 147–188.
568 Platt, U., Stutz, J., 2008. Differential optical absorption spectroscopy: Principles and
569 applications, First Edit. ed. Springer.
570 Serdyuchenko, A., Gorshelev, V., Weber, M., Chehade, W., Burrows, J.P., 2014. High
571 spectral resolution ozone absorption cross-sections – Part 2: Temperature
572 dependence. Atmos. Meas. Tech. 7, 625–636. https://doi.org/10.5194/amt-7-625-2014
573 Setyan, A., Flament, P., Locoge, N., Deboudt, K., Riffault, V., Alleman, L.Y., Schoemaecker,
574 C., Arndt, J., Augustin, P., Healy, R.M., Wenger, J.C., Cazier, F., Delbarre, H.,
575 Dewaele, D., Dewalle, P., Fourmentin, M., Genevray, P., Gengembre, C., Leonardis, T.,
576 Marris, H., Mbengue, S., 2019. Investigation on the near-field evolution of industrial
577 plumes from metalworking activities. Sci. Total Environ. 668, 443–456.
578 https://doi.org/10.1016/j.scitotenv.2019.02.399
579 Seyler, A., Wittrock, F., Kattner, L., Mathieu-Üffing, B., Peters, E., Richter, A., Schmolke,
580 S., Burrows, J.P., 2017. Monitoring shipping emissions in the German Bight using
581 MAX-DOAS measurements. Atmos. Chem. Phys. 17, 10997–11023.
582 https://doi.org/10.5194/acp-17-10997-2017
583 Stein, A.F., Draxler, R.R., Rolph, G.D., Stunder, B.J.B., Cohen, M.D., Ngan, F., 2015.
584 Noaa's hysplit atmospheric transport and dispersion modeling system. Bull. Am.
585 Meteorol. Soc. 96, 2059–2077. https://doi.org/10.1175/BAMS-D-14-00110.1
586 Stroud, C., Madronich, S., Atlas, E., Ridley, B., Flocke, F., Weinheimer, A., Talbot, B.,
587 Fried, A., Wert, B., Shetter, R., Lefer, B., Coffey, M., Heikes, B., Blake, D., 2003.

588 Photochemistry in the arctic free troposphere: NOx budget and the role of odd nitrogen
589 reservoir recycling. Atmos. Environ. 37, 3351–3364. https://doi.org/10.1016/S1352-
590 2310(03)00353-4
591 Stutz, J., Kim, E.S., Platt, U., Bruno, P., Perrino, C., Febo, A., 2000. UV-visible absorption
592 cross sections of nitrous acid. J. Geophys. Res. 105, 14585–14592.
593 Tang, L., Ramacher, M.O.P., Moldanová, J., Matthias, V., Karl, M., Fridell, E., Johansson,
594 L., 2020. The impact of ship emissions on air quality and human health in the
595 Gothenburg area – Part II: Scenarios for 2040. Atmos. Chem. Phys. 20, 10667–10686.
596 https://doi.org/10.5194/acp-20-10667-2020
597 Thalman, R., Volkamer, R.A., 2013. Temperature Dependent Absorption Cross-Sections of
598 O2-O2 collision pairs between 340 and 630 nm and at atmospherically relevant pressure.
599 Phys. Chem. Chem. Phys. 15, 15371–15381. https://doi.org/10.1039/C3CP50968K
600 Twomey, S., 1977. The Influence of Pollution on the Shortwave Albedo of Clouds. J. Atmos.
601 Sci. 34, 1149–1152. https://doi.org/10.1175/1520-
602 0469(1977)034<1149:TIOPOT>2.0.CO;2
603 Vandaele, A.C., Hermans, C., Simon, P.C., Carleer, M.R., Colin, R., Fally, S., Merienne,
604 M.F., Jenouvrier, A., Coquartii, B., Colins, R., Fally, F., Coquart, B., 1998.
605 Measurements of NO2 absorption cross-sections at 42000 cm-1 to 10000 cm-1 (238-
606 1000 nm) at 220 K and 294 K. J. Quant. Spectrosc. Radiat. Transf. 59, 171–184.
607 Viana, M., Hammingh, P., Colette, A., Querol, X., Degraeuwe, B., Vlieger, I. de, van
608 Aardenne, J., 2014. Impact of maritime transport emissions on coastal air quality in
609 Europe. Atmos. Environ. 90, 96–105. https://doi.org/10.1016/j.atmosenv.2014.03.046
610 World Health Organization, 2021. WHO global air quality guidelines. Particulate matter
611 (PM2.5 and PM10), ozone, nitrogen dioxide, sulfur dioxide and carbon monoxide.
612 Licence: CC BY-NC-SA 3.0 IGO, Geneva.

Zhang, S., Tison, E., Dusanter, S., Beaugard, C., Gengembre, C., Augustin, P., Fourmentin, M., Delbarre, H., Riffault, V., 2021. Near real-time PM1 chemical composition measurements at a French urban background and coastal site under industrial influence over more than a year: Temporal variability and assessment of sulfur-containing emissions. Atmos. Environ. 244. https://doi.org/10.1016/j.atmosenv.2020.117960

Tables:

Table 1: DOAS retrieval settings for the four species retrieved as a part of this study.

Trace gas	Cross-section Molecule	Reference
O_4 and NO_2 (338-370 nm); Polynomial order 5; Predefined offset: Constant; Orthobase order: 2		
NO_2 294K	Diff XS; Conv Std.	(Vandaele et al., 1998)
NO_2 220K	Ortho to NO2 294K; Conv Std.	(Vandaele et al., 1998)
O_3 223K	Ortho to O3 273K; Conv Std.	(Serdyuchenko et al., 2014)
O_3 243K	Diff XS; Conv Std.	(Serdyuchenko et al., 2014)
O_4 293K	None; Conv Std.	(Thalman and Volkamer, 2013)
CH2O 298K	Diff XS; Conv Std.	(Meller and Moortgat, 2000)
BrO 223K	Diff XS; Conv Std.	(Fleischmann et al., 2004)
HONO 298K	Diff XS; Conv Std.	(Stutz et al., 2000)
Ring	Diff XS; Conv Ring	(Chance and Kurucz, 2010)
HCHO (312.5-359 nm); Polynomial order 5; Predefined offset: Constant; Orthobase order: 2		
HCHO_298K	None; Convolve std	(Meller and Moortgat, 2000)
BrO_223K	Diff XS; Convolve std	(Fleischmann et al., 2004)
NO_2_294K	Diff Xs; Convolve I_0 (1e17) + Pukite	(Vandaele et al., 1998)
NO_2_220K	Ortho to NO_2_294K; Convolve I_0 (1e17)	(Vandaele et al., 1998)
O_3_223K	Diff XS; Convolve I_0 (1e20) + Pukite	(Serdyuchenko et al., 2014)
O_3_243K	Ortho to O_3 223K; Convolve I_0 (1e20)	(Serdyuchenko et al., 2014)
O_4_293K	None; Convolve std	(Thalman and Volkamer, 2013)
HONO_298K	Diff XS; Convolve std	(Stutz et al., 2000)
Ring	Diff XS; Convolve to Ring	(Chance and Kurucz, 2010)
SO_2 (307.7-330 nm); Polynomial order 5; Predefined offset: Constant; Orthobase order: 2		
SO_2_293K	Diff XS; Conv Std.	(Bogumil et al., 2003)
HCHO_298K	None; Convolve std	(Meller and Moortgat, 2000)
BrO_223K	Diff XS; Convolve std	(Fleischmann et al., 2004)
NO_2_294K	Diff XS; Convolve I_0 (1e17) + Pukite	(Vandaele et al., 1998)
NO_2_220K	Ortho to NO2 294K; Convolve I_0 (1e17)	(Vandaele et al., 1998)
O_3_223K	Diff XS; Convolve I_0 (1e20) + Pukite	(Serdyuchenko et al., 2014)
O_3_273K	Ortho to O_3 223K; Convolve I_0 (1e20)	(Serdyuchenko et al., 2014)
Ring	Convolve to Ring	(Chance and Kurucz, 2010)

Figures

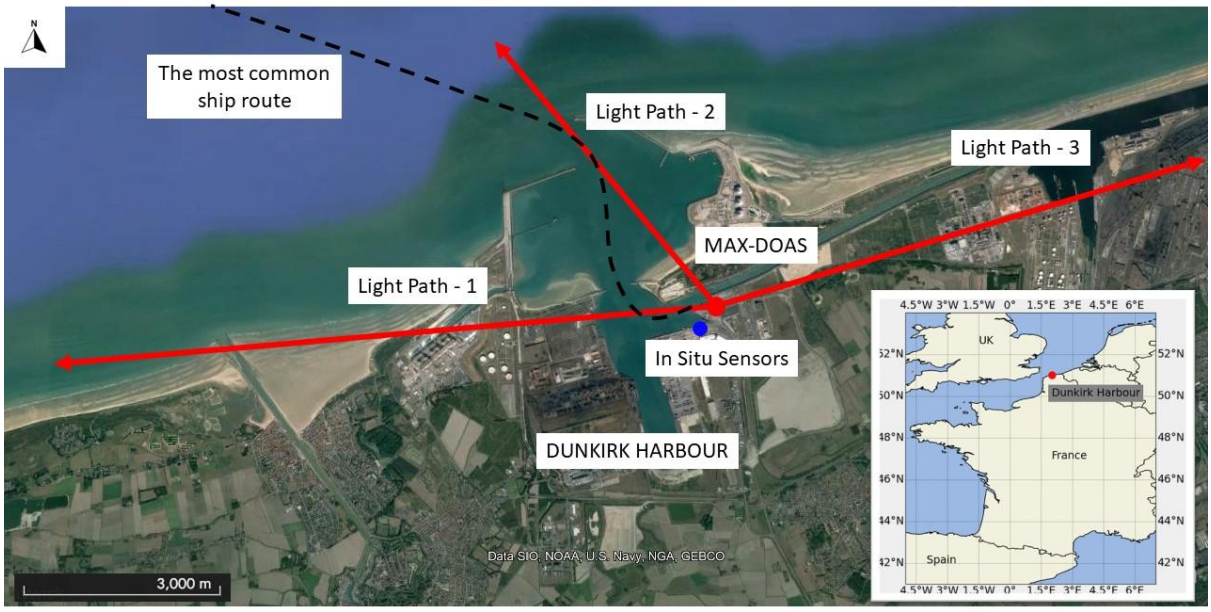

Figure 1: Map showing the location of the MAX-DOAS instrument (red dot) during the field campaign, along with the three light paths used during the study. The first light path pointed westward (azimuth 262°), to the north of the ferry dock, the second light path looked over the harbour opening towards the open ocean (azimuth 306°), and the third path looked over an industrial area to the east of the harbour (azimuth 60°). The location of the in situ sensors is shown as a blue dot. Please note that the lines are indicative of the viewing direction and not the actual path length for the observations, which are variable according to environmental conditions. The most common ship route for the regular ferries docking in the harbour is indicated (black dashed line). Satellite image: Google Earth.

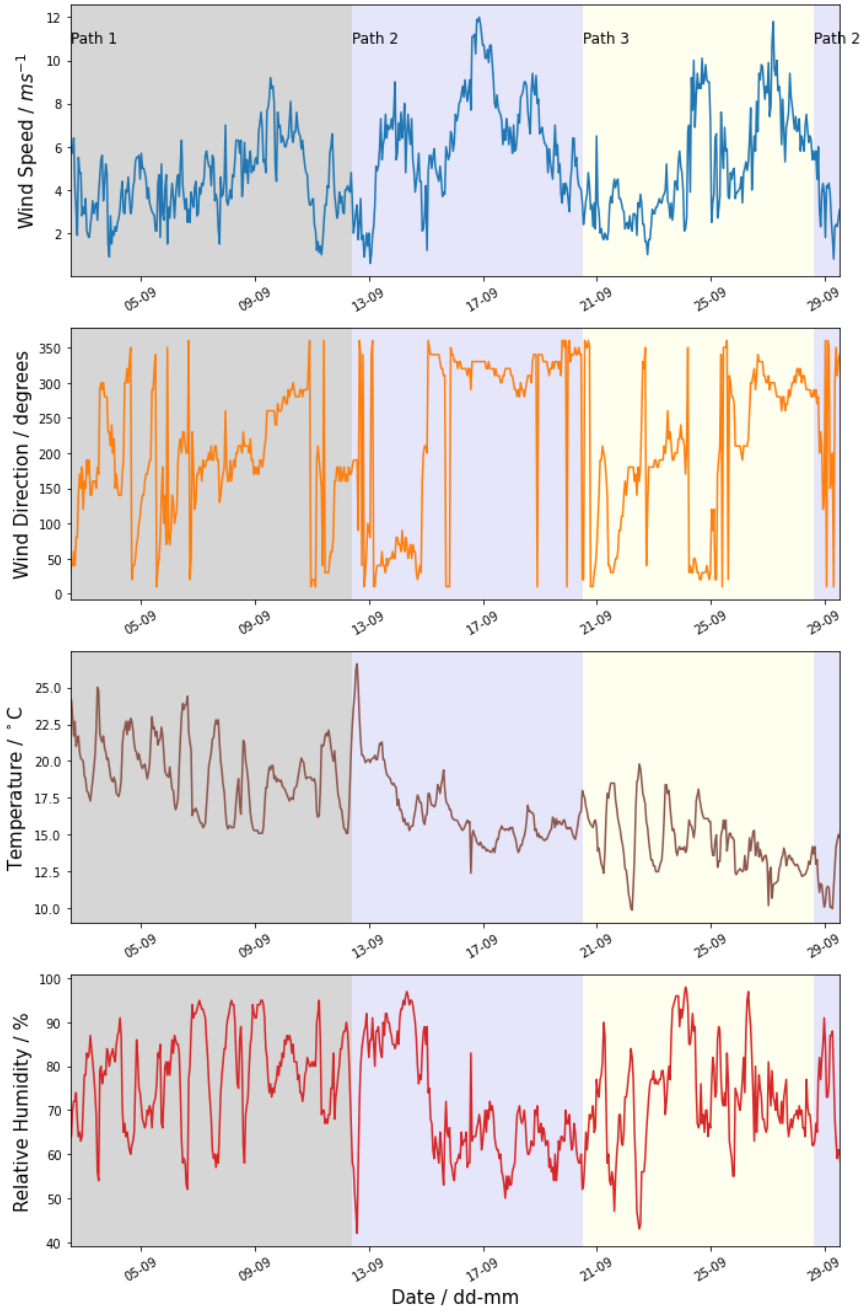

634

635 **Figure 2**: Meteorological parameters observed during the field campaign. The data are

636 shaded according to the different light paths used during the study.

637

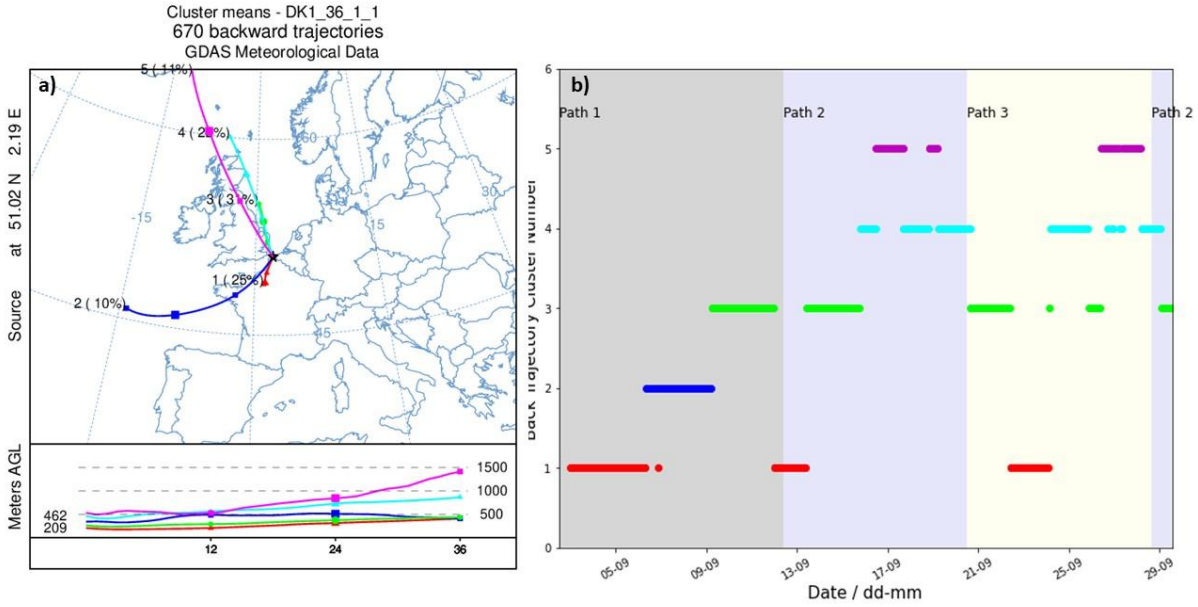

638

639 **Figure 3**: Air mass back trajectories observed during the field campaign. Panel a) represents
640 the means of the five different types of back trajectories observed during the campaign, and
641 panel b) shows the individual hourly back trajectories in the same colour scheme as (a). The
642 data are shaded according to the different light paths used during the study.

643

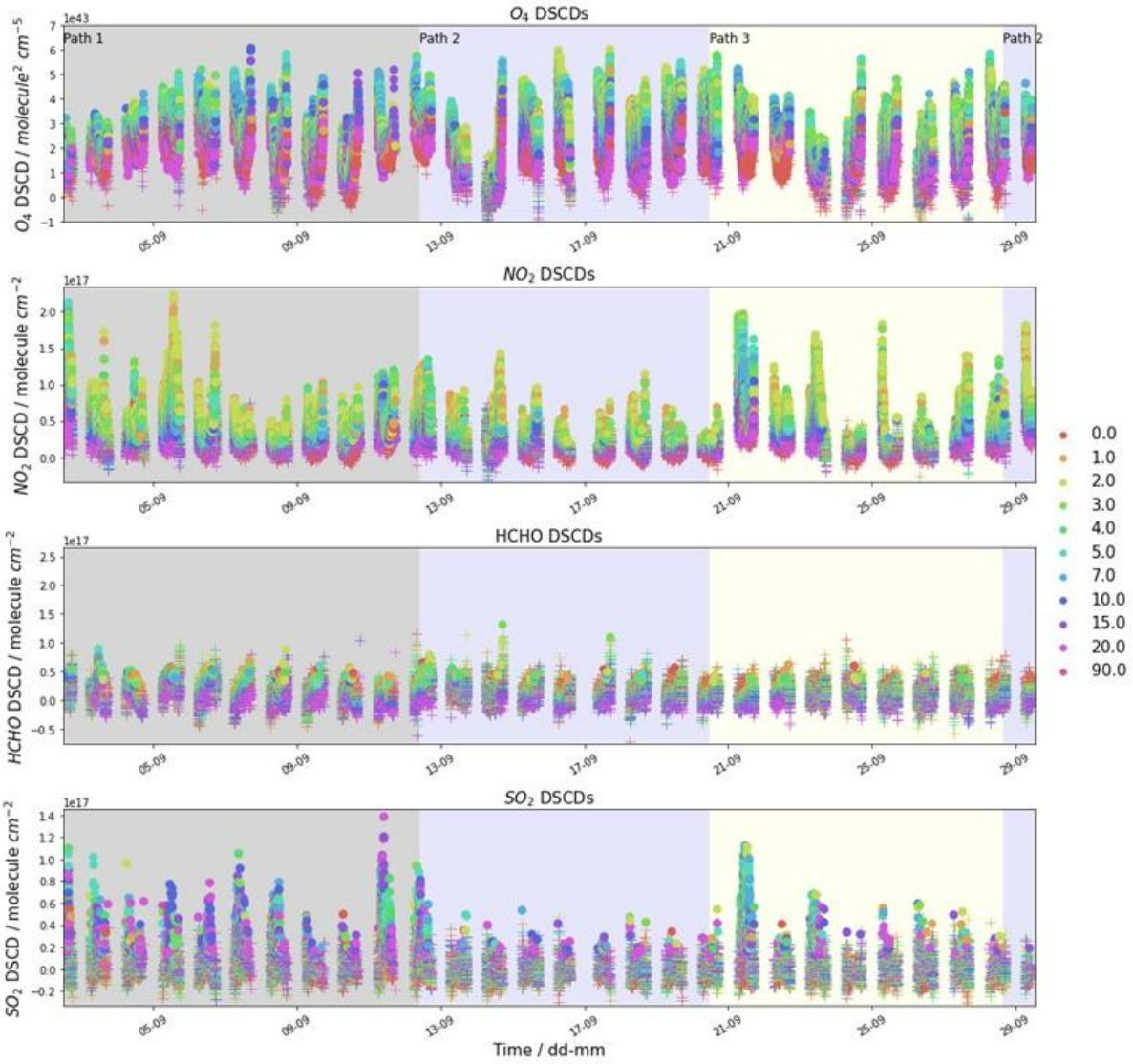

644

645 **Figure 4**: Timeseries of DSCDs according to the observed elevation angles for the different
646 species during the field campaign. The filled circles show the data above the 2 σ detection
647 limit of the instrument, color-coded according to elevation angles, while the '+' symbols
648 represent data below the detection limit. The data are shaded according to the different light
649 paths used during the study.

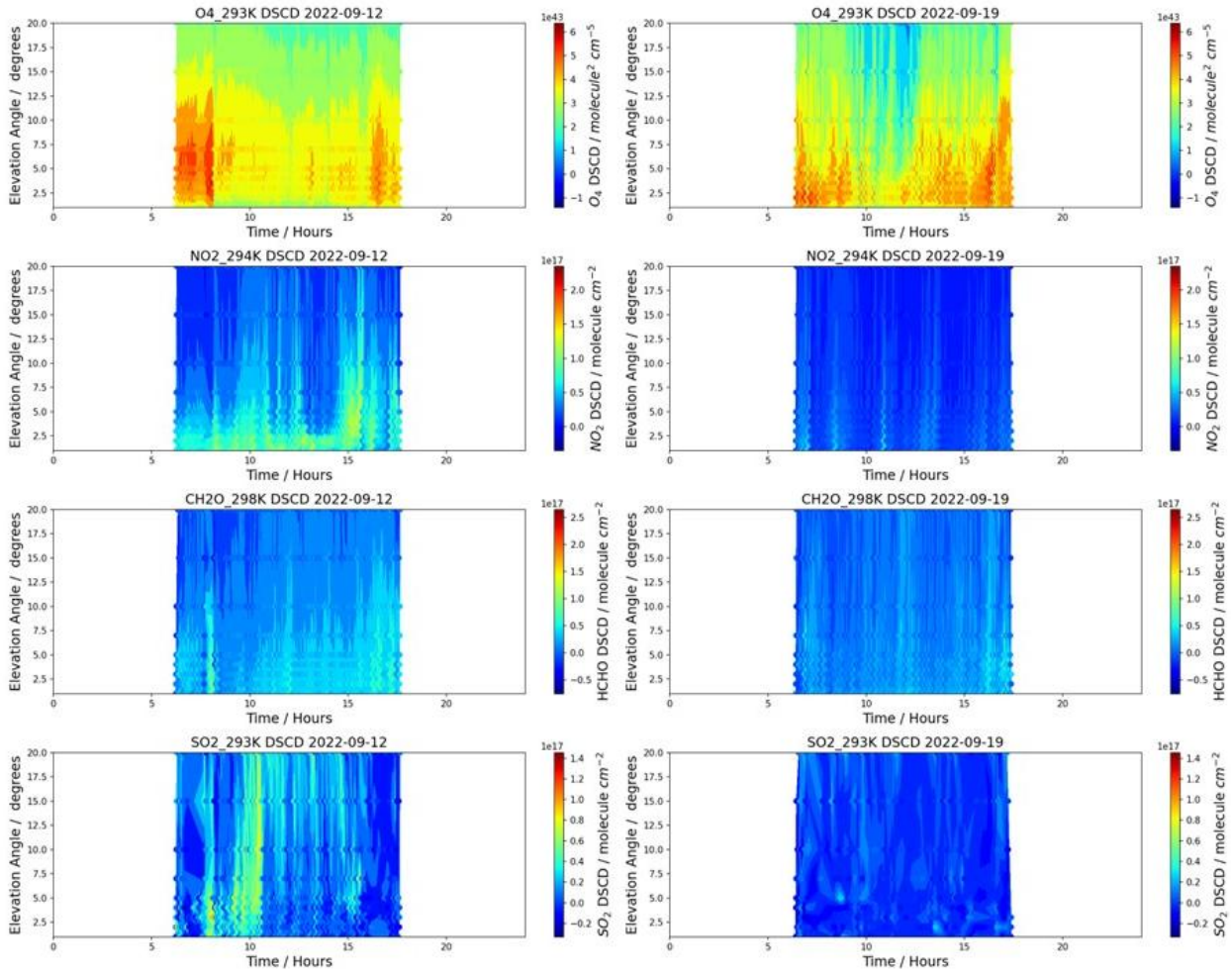

650

651 **Figure 5:** DSCD values of O_4, NO_2, HCHO, and SO_2 according to elevation angles observed

652 during two example days (12th and 19th of September 2022). Both observations were made

653 along light path 2, towards the north over the North Sea.

654

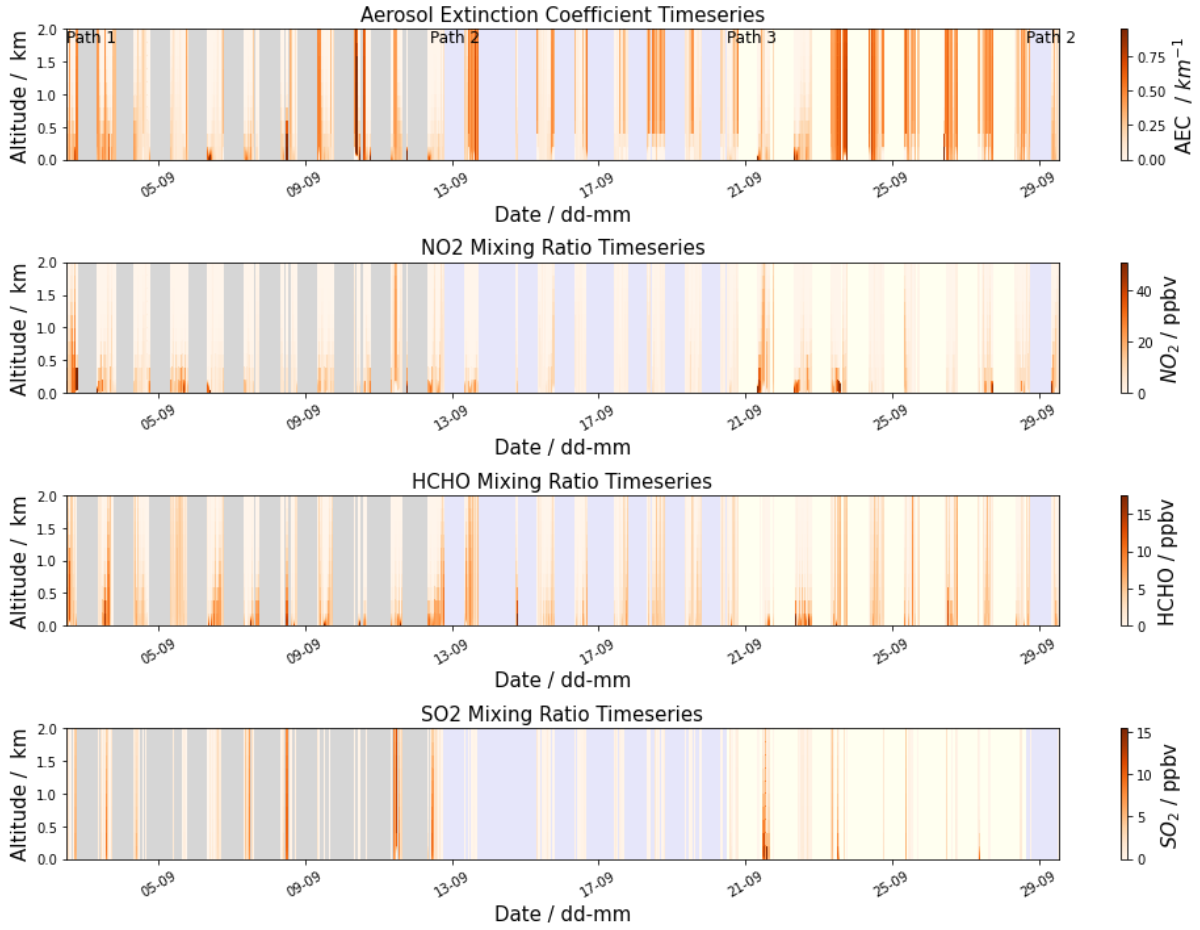

655

656 **Figure 6**: Timeseries of vertical profiles of aerosol extinction coefficients (AEC) and NO_2,
657 HCHO and SO_2 mixing ratios are shown. The data are shaded according to the different light
658 paths used during the study. Note that presence of elevated concentrations at higher altitude
659 (>500 m) should be treated with caution due to multiple scattering effects of clouds.

660

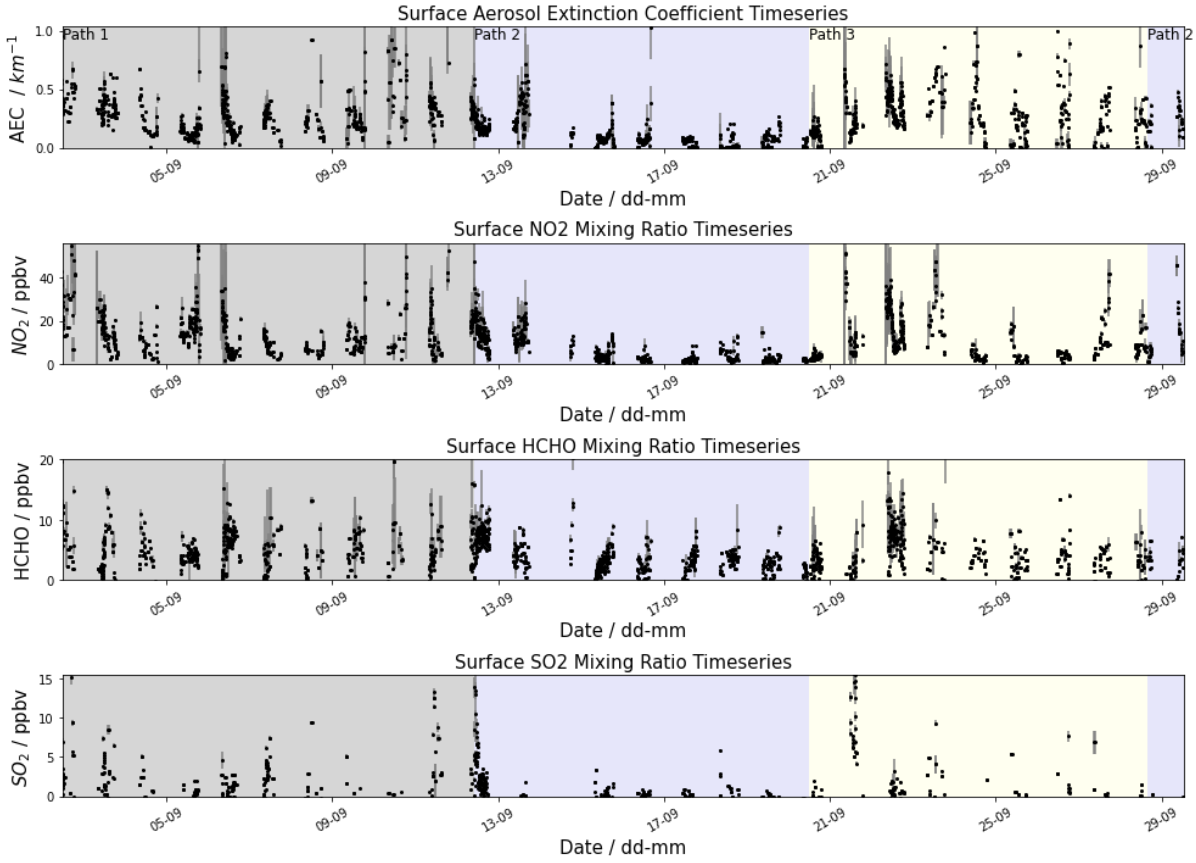

661

662 **Figure 7:** Timeseries of surface AECs and NO_2, HCHO and SO_2 mixing ratios are shown.

663 The data are shaded according to the different light paths used during the study.

664

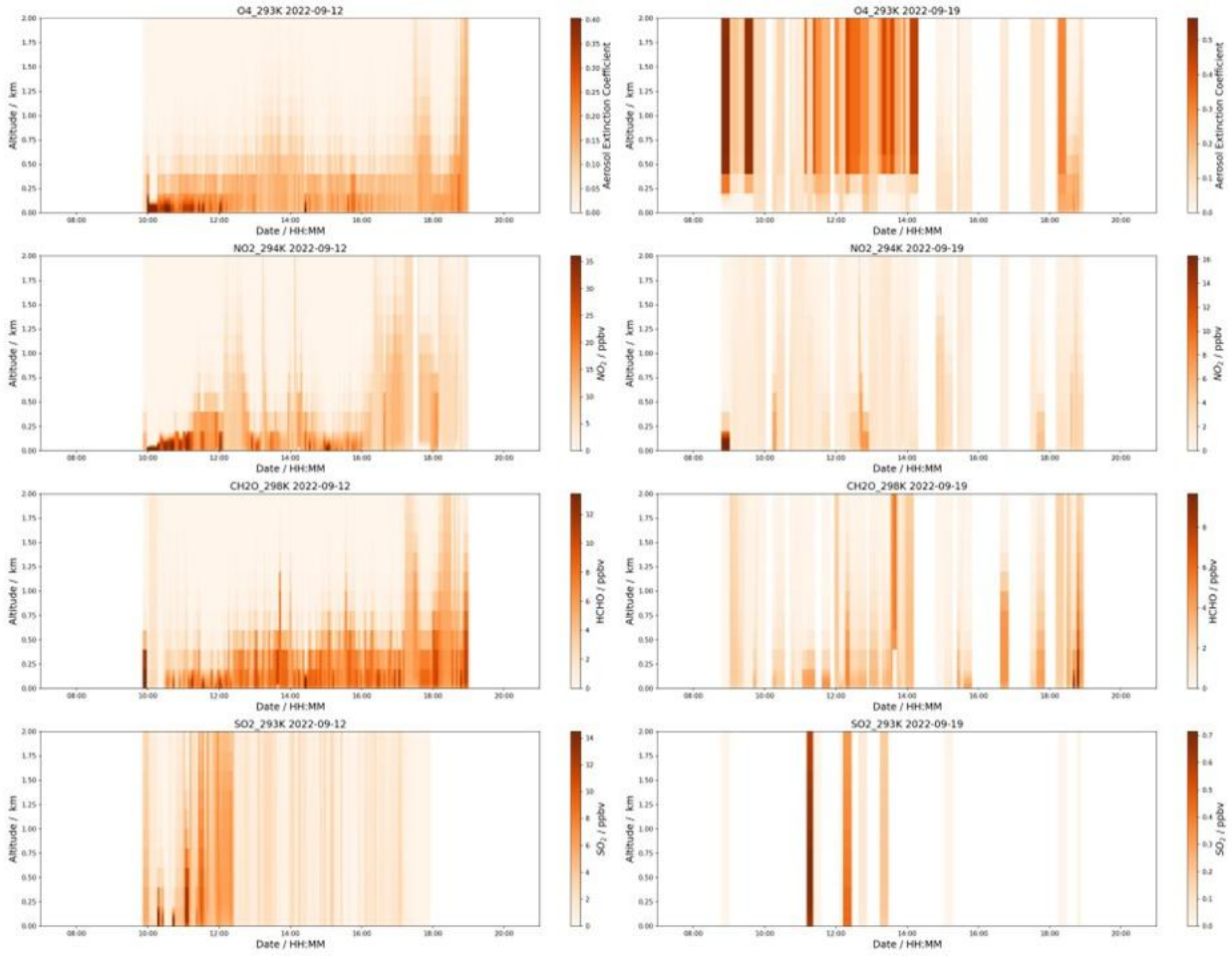

665

666 **Figure 8:** Vertical profiles of AEC, NO_2, HCHO and SO_2 mixing ratios during two example
667 days (12^{th} and 19^{th} of September 2022). Both observations were made along light path 2,
668 towards the north over the North Sea.

669

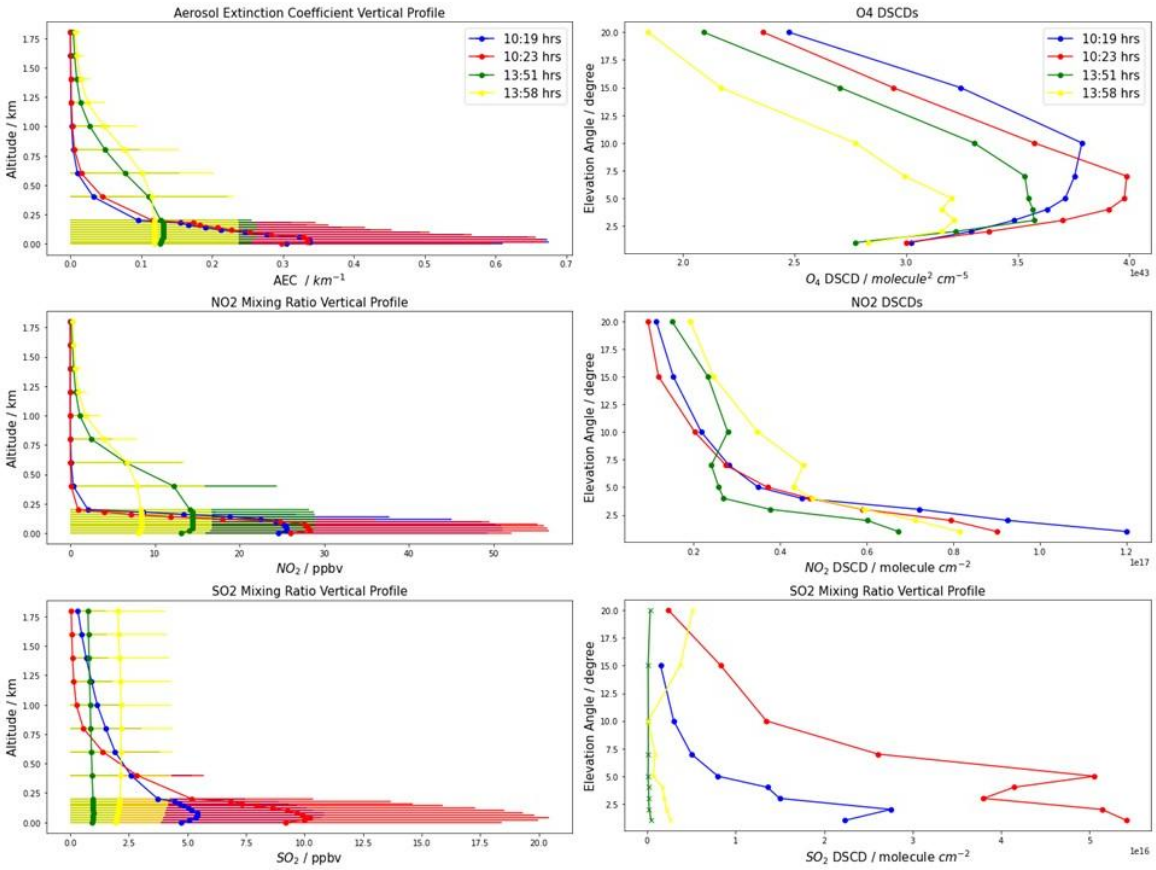

670

671 **Figure 9:** (Left) Comparison of vertical profiles of AEC, and NO_2 and SO_2 mixing ratios
672 when ship plumes were observed (blue & red symbols) with those when no ship plume was
673 observed (green & yellow symbols) from 12th September 2022. An enhancement in the lower
674 boundary layer is visible. (Right) Corresponding DSCDs for O_4, NO_2 and SO_2 from the same
675 MAX-DOAS scans showed larger DSCDs when the instrument sampled the ship plume. Note
676 that the SO_2 DSCDs scans marked with '×' were below the detection limit.

677

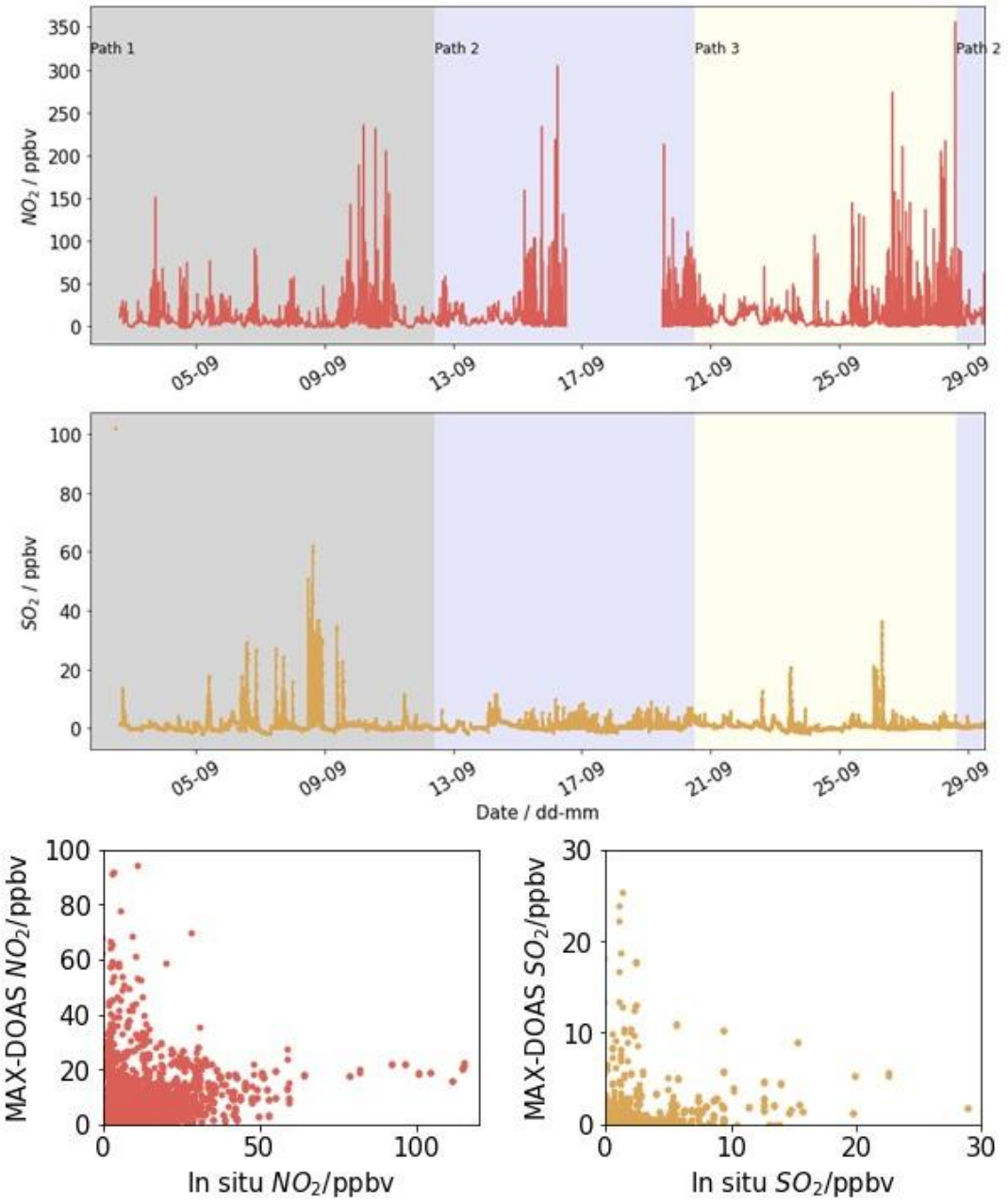

678

679 **Figure 10:** The timeseries of surface NO_2 and SO_2 mixing ratios as observed by the in situ
680 sensors is shown. The data are shaded according to the different light paths used during the
681 study. The bottom two panels show the comparison between the MAX-DOAS (lowest 200 m)
682 and in situ surface mixing ratios, showing that the two instruments did not always sample the
683 same air masses.

684

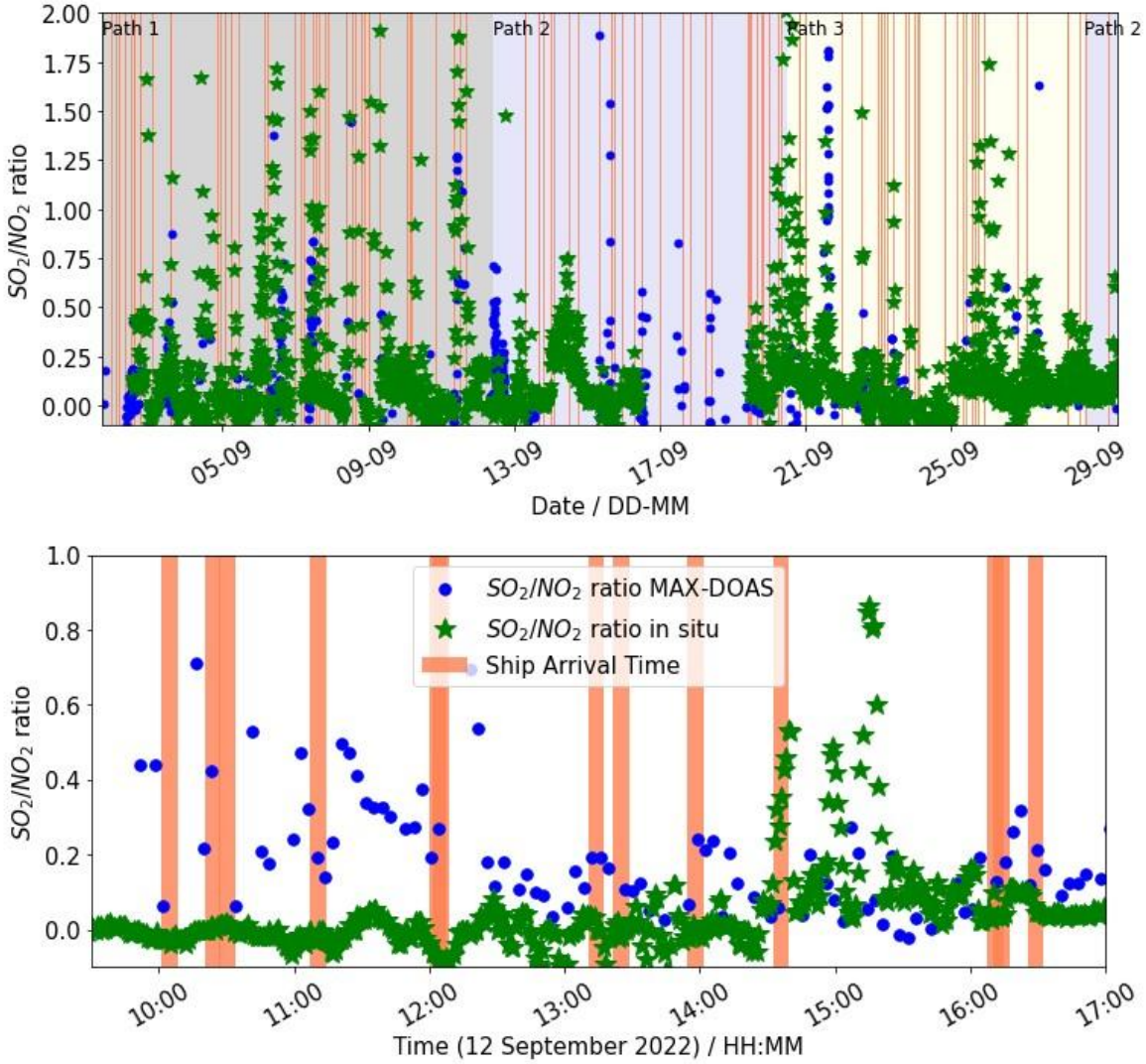

685

686 **Figure 11:** SO_2/NO_2 ratio observed throughout the campaign by the MAX-DOAS (blue
687 dots), in situ instruments (green asterisks) and ship arrival times (red bars). Not all the ships
688 stayed for the same duration, and their engines were on for variable periods. Hence, arrival
689 times indicate ship emissions but do not cover the entire period when the MAX-DOAS
690 sampled the ship plume. An increase in the ratio is observed in the MAX-DOAS every time a
691 ship comes into the harbour but not in the in situ observations, which depends on the local
692 wind direction. The bottom plot shows the zoomed-in figure for 12th September 2022.

693